

---

# Beyond *Bare* Queries: Open-Vocabulary Object Retrieval with 3D Scene Graph

---

Sergey Linok<sup>1\*</sup> Tatiana Zemskova<sup>1,2\*</sup>  
Svetlana Ladanova<sup>1</sup> Roman Titkov<sup>1</sup> Dmitry Yudin<sup>1,2</sup>  
<sup>1</sup>MIPT <sup>2</sup>AIRI  
{linok.sa,ladanova.sv,titkov.re}@phystech.edu  
{yudin,zemskova}@airi.net

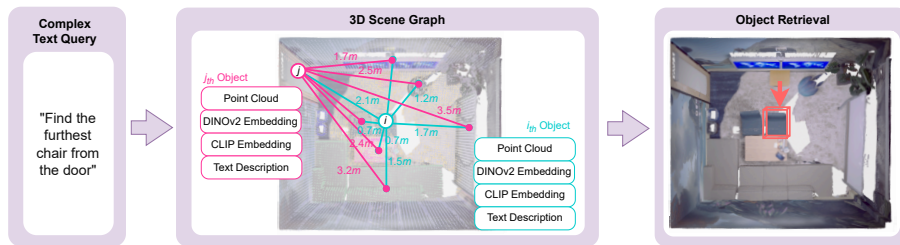


Figure 1: Proposed *BBQ* approach leverages foundation models for high-performance construction of an object-centric class-agnostic 3D map of a static indoor environment from a sequence of RGB-D frames with known camera poses and calibration. To perform scene understanding, we represent surroundings as a set of nodes with spatial relations. Utilizing a designed *deductive* scene reasoning algorithm, our method closes the gap in human-to-agent communication by enabling free-form natural language interaction with a scene-aware large language model.

## Abstract

Locating objects referred to in natural language poses a significant challenge for autonomous agents. Existing CLIP-based open-vocabulary methods successfully perform 3D object retrieval with simple (*bare*) queries but cannot cope with ambiguous descriptions that demand an understanding of object relations. To tackle this problem, we propose a modular approach called *BBQ* (Beyond *Bare* Queries), which constructs 3D scene spatial graph representation with metric edges and utilizes a large language model as a human-to-agent interface through our *deductive* scene reasoning algorithm. *BBQ* employs robust DINO-powered associations to form 3D objects, an advanced raycasting algorithm to project them to 2D, and a vision-language model to describe them as graph nodes. On Replica and ScanNet datasets, we show that the designed method accurately constructs 3D object-centric maps. We have demonstrated that their quality takes a leading place for open-vocabulary 3D semantic segmentation against other zero-shot methods. Also, we show that leveraging spatial relations is especially effective for scenes containing multiple entities of the same semantic class. On Sr3D and Nr3D benchmarks, our deductive approach demonstrates a significant improvement, enabling retrieving objects by complex queries compared to other state-of-the-art methods. Considering our design solutions, we achieved a processing speed approximately  $\times 3$  times faster than the closest analog. This promising performance enables our approach for usage in applied intelligent robotics projects. We make the code publicly available at [linokc.github.io/bbq/](https://github.com/linokc/bbq/).

# 1 Introduction

Open-vocabulary perception is a primary challenge for next-level AI-powered autonomous agents. For example, finding a referred object by a complex text query in a surrounding 3D space full of semantically identical distractors remains an open question.

To marry vision and text modalities CLIP-based encoders [1–6] have been firmly established as a classic approach that predicts the most relevant text snippet in natural language to a given 2D image. These methods do not require additional training or fine-tuning for small domain shifts, thus allowing effective zero-shot use as foundation models on new data. However, due to being primarily trained on image-class label pairs, such models lack an understanding of complex text queries, visual relations, general reasoning ability, and spatial awareness. To address these gaps state-of-the-art methods propose various architectures to consume different visual prompts like points, boxes, masks, etc., alongside with rich text descriptions and auxiliary annotations [7–19].

To work with 3D data the big question arises: how to effectively encode visual embeddings of the environment? For open-vocabulary understanding most modern methods project 2D foundation features to 3D [20–26], treat accumulated RGB-D images as a point cloud and perform pointwise distillation [27, 28], combine both approaches [29–36], or utilize advanced scene-specific representations like NeRF [37–41] and Gaussian Splatting [42–44]. To perceive a surrounding 3D environment both trainable and parameter-free techniques are applied.

Integrating a large language model (LLM) into a perception pipeline can provide a source of world knowledge and generalizable foundational features, enabling complex text understanding and reasoning. To add the ability to perceive visual modality, this group of methods utilizes pretrained frozen CLIP-based image encoders. With the help of comprehensive natural language descriptions and additional visual prompts, visual large language models (vLLM) [45–50] perform instruction-tuning of projection layers on the next prediction token using their original auto-regressive training objective.

In our research, we particularly focus on parameter-free techniques that exploit the generalization ability of pretrained frozen models to perform 3D scene open-vocabulary understanding in a zero-shot manner. But what are the challenges for state-of-the-art methods in this field?

**The first challenge** for the aforementioned 3D methods is the difficulty in accumulating reliable visual representations because, as they rely on local 2D proposals [51, 52] that only partially cover objects in images. 3D proposal generators are designed to improve this limitation. However, they reduce the scope of applications in the real world as they are distilled versions of 2D proposal methods or supervised instance segmentation models [53, 54] and require full scene point cloud accumulation. Promising ideas are the 3D object-centric map construction from a sequence and 2D projection to the best-view frame for visual encoding. However, both ideas struggle with time consumption in their current implementations: Gu et al. [24] utilizes CLIP embeddings both for visual encoding and proposals-to-objects accumulation thus requiring to call model *for each* incoming detection *in each 2D frame*, and Takmaz et al. [31] has to project each object back to *each* frame in a sequence to calculate best visibility score. To face this challenge we explicitly separate the 3D objects map process from object visual encoding. Self-supervised DINO image embeddings mark themselves as robust discriminative features that are sufficient for strong 2.5D understanding [55]. For each frame, we extract these deep features and employ fast DINO-based proposals-to-object accumulation (Sec. 3.1). At the end of a sequence to select a pose to project we perform the designed multiview clusterization technique before conducting a best-view search (Sec. 3.2). That reduces time consumption to a matter of milliseconds and in practice proves no quality loss (Sec. 4.1). We provide more information about our design’s influence on performance speed in Section 4.3.

**The second challenge** is to preserve scene spatial awareness in object relations. To cope with this challenge graph-based approaches have been presented [50, 33, 56–60]. However, they rely on training neural networks from supervision signals. Gu et al. [24] proposes an idea to utilize LLM to predict a finite set of edge types (in, on) based on object captions and box coordinates. In contrast, we designed cheap to construct spatial-aware 3D scene representation as a graph with metric edges (Sec. 3.3 and Sec. 3.4). This approach does not need heavy and overwhelming large language model calls and is not limited by natural language edge definitions.

However, such straightforward method raises **the third challenge**: how to effectively incorporate 3D scene representation into a large language model? Inspired by the chain-of-thoughts technique we

devise the idea of LLM *deductive* reasoning (Sec. 3.5). Experiments on challenging benchmarks for 3D object retrieval show the advantage of integration with large language models over a multimodal CLIP map and highlight how the language model benefits from the suggested strategy (Sec. 4.2).

**To summarize**, the contributions of this paper include:

- high-performance DINO-based 3D object-centric map accumulation approach from a sequence of RGB-D images;
- 2D *best* view selection strategy based on multiview clusterization for reach and comprehensive object visual captioning;
- cheap to construct and descriptive effective 3D scene graph representation with metric edges;
- *deductive* scene reasoning algorithm to utilize our scene graph representation with large language model for open-vocabulary referred objects retrieval;
- integration of these capabilities in a single modular approach called BBQ (Beyond Bare Queries). We make the code publicly available at [linukc.github.io/bbq/](https://github.com/linukc/bbq).

## 2 Related work

Parameter-free methods that perform 3D scene open-vocabulary understanding in a zero-shot manner can be broadly categorized into four groups based on the scene representation type: point-based [22, 20], pointcloud-based [31, 29], object-centric [24, 23, 36], tsdf-based [25]. We select the most modern and promising works from each group and discuss our key differences.

*ConceptFusion* by Jatavallabhula et al. [22] proposes an open-set multimodal 3D mapping technique that computes pixel-aligned 2D foundation features and fuses them into a 3D point map. They use SAM [51] model to generate class-agnostic object masks and OpenClip [61] to assign visual embeddings. However, we noticed, that assigning the same embedding for each pixel on the mask creates unnecessary duplication that leads to huge memory usage in large scenes. Additionally, fusing data from all frames add unnecessary noise to an object representation from visible but unrecognizable views. In contrast, our method build upon an object-centric paradigm: for each object in the resulted 3D scene, we calculate only one CLIP descriptor, which we compute using our *best* view projection.

*OpenMask3D* by Takmaz et al. [31] leverages 3D mask proposals powered by the instance segmentation model Mask3D [53] to select topK views from an RGB-D sequence for CLIP-based per mask 2D feature extraction. This gravely limits the method’s applications due to the necessity of having such a pretrained model on the desired data domain. It also leads to the necessity of utilizing SAM [51] with an advanced outliers removal procedure for selected views mask refinement. In contrast we fully rely on SAM [51] proposals and accumulate objects from 2D rather 3D proposals. To remove noise from inaccurate masks we apply DBSCAN over a projected object 3D point cloud.

*OpenFusion* by Yamazaki et al. [25] builds the pipeline upon TSDF to achieve effective close to real-time 3D scene reconstruction with approximately 4.5 FPS. Unlike the widely adopted CLIP-based encoders authors utilized the modern SEEM [18] model to produce region-level aligned image features. This aims to eliminate the need for the expensive class agnostic mask proposal generator in two-stage setups like *ConceptFusion* [22]. Despite great achievements, it is important to highlight that *OpenFusion*’s scene representation lacks spatial relations between objects. This leads to behavior where all semantically close objects will be spotted. In our work to achieve spatial relation awareness, we build a 3D map in an object-centric manner considering each object as a node in a metric edge graph.

The closest approach to BBQ is *ConceptGraphs* by Gu et al. [24]. As in our pipeline, the authors leverage SAM [51] 2D proposals and accumulate 3D objects from frames in a sequence. However, we do not rely on CLIP visual embeddings for the objects association process but rather utilize DINO [62, 63] descriptors that we calculate by calling the model once per image instead of calling CLIP per proposal mask. These descriptors are well studied and proven as robust spatially aware features that can be leveraged for associating identical objects on image frames [55, 64–66]. A significant difference between methods lies in the process of object view selection: *ConceptGraphs* choose between only preserved local 2D masks, which tend to local part description or even complete misinterpretation. In contrast, we select the *best* object view with our multiview clusterization and after performing raycasting achieve an instance mask for captioning. This allows us to significantly

better represent objects for visual understanding. Also, *ConceptGraphs*, to our knowledge, is one of the first methods that discuss graph construction without the need for any training for scene representation in LLM. They utilize object-centric map representation to create image captioning for each object/node and consider on/in edge generation with language model by text descriptions. Unfortunately, the authors performed their research with the proprietary ChatGPT-4 model, which is great but limits the capability of broad usage. Moreover, scene representation in LLM is only theoretically discussed but not utilized for experiments. Inspired by the described idea we perform detailed studies on how to effectively encode spatial relations between objects in edges without the limit of natural language expression and show the results of our *deductive* reasoning technique over metric edge graph on challenging Sr3D [67] and Nr3D [67] benchmarks where our approach with a large language model demonstrates a significant improvement, enabling retrieving objects surrounded by semantic distractors by complex queries.

### 3 Method

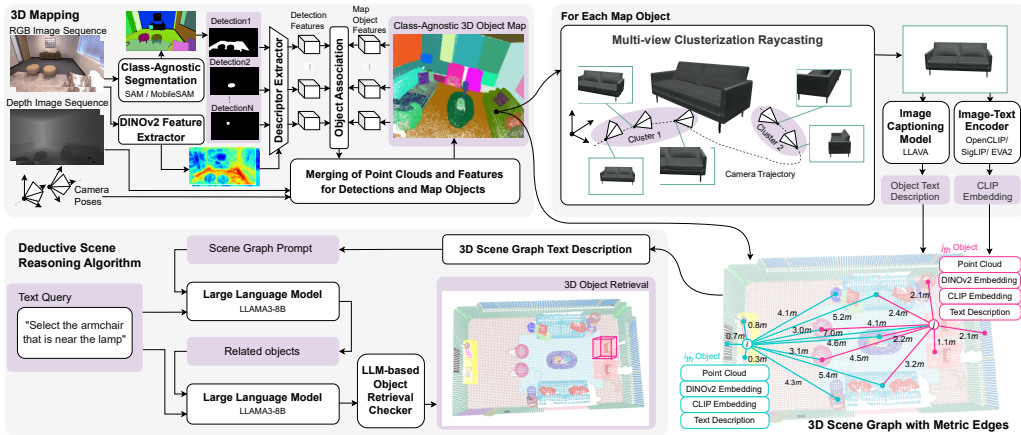


Figure 2: An object-centric, class-agnostic 3D map is iteratively constructed from a sequence of RGB-D camera frames and their poses by associating 2D SAM mask proposals with 3D objects with deep DINO visual features and spatial constraints (Sec. 3.1). To visually represent objects after building the map, we select the *best* view based on the largest projected mask from  $K$  cluster centroids that represent areas of object observations (Sec. 3.2). We leverage LLaVA [48] to describe object visual properties (Sec. 3.3). With the node’s text descriptions, spatial locations, and metric edges (Sec. 3.4) we utilize LLM in our *deductive* reasoning algorithm (Sec. 3.5) to perform a 3D object retrieval task.

#### 3.1 Object-centric 3D map construction

For each input RGB-D frame  $I$  with a resolution  $H \times W$  pretrained frozen model extract set of 2D proposal boolean masks  $M \in \mathbb{R}^{H \times W}$  and DINO embeddings  $E_{DINO} \in \mathbb{R}^{H/s \times W/s \times dim}$ , where  $s$  is DINO transformer patch *stride*. For  $M$  we experimented with original SAM [51] and fast MobileSAMv2 [52], for  $E_{DINO}$ , we examined DINO [62] and DINOv2 [63] with registers [68].

After a series of filtration checks to discard low confidence, small or too large regions each passed mask  $m$  is represented as point cloud  $p \in \mathbb{R}^{N \times 3}$ , where  $N$  - number of points in mask that we project based of depth information, pose and camera calibration. To point cloud  $p$  we additionally apply DBSCAN to remove noise from inaccurate 2D proposal  $m$ . Associated descriptor  $d \in \mathbb{R}^{dim}$  is extracted from  $E_{DINO}$  by averaging all features in interpolated to  $R^{H/s \times W/s}$  mask  $m$ . Each frame  $I$  from sequence of images is represented by detection set  $\{(p_k, d_k) \mid k \in (1, \dots, K)\}$ , where  $K$  - number of selected proposals.

To construct a class-agnostic object-centric 3D map on each frame we perform an association process between incoming detections set and objects on the scene. For the first frame, we simply initialize

objects as detections. Association process consists of finding visual cosine similarities between all intersected instances. If for  $j$ -th detection  $CosineSimilarity(d_j, d_i)$  lower than visual threshold  $\sigma_{vis}$  for every object  $i$ , we initialize this detection as a new object, else merge with closest by cosine similarity. During merging process we combine point clouds, increase number of detections for object, add frame index for future 3D to 2D projection search and most importantly update object visual descriptor with our sliding technique:  $d_i = 0.8d_j + 0.2d_i$ . Assigning a higher weight to incoming descriptors leverages the capability of DINO features to effectively identify correspondences between local frames while preserving information for objects merging. To reduce the growing number of objects that appear after unsuccessful association each  $m$ -th iteration object merging with lower  $\sigma_{vis}$  and spatial overlap check is called. Two descriptors in this case simply averaged. After object map construction we perform the postprocessing step: filter objects to discard outliers and merge objects based on spatial overlap.

### 3.2 Object best view 3D to 2D projection

Because performing the raycasting procedure for all poses is time-consuming, we decided to cluster 3D camera coordinates  $P_i = \{(x, y, z)_q \mid q \in (1, \dots, Q)\}$  from  $Q$  viewpoints where we observed the object  $o_i$ , to  $L$  groups. We consider  $L$  as an important BBQ hyperparameter. Then, we select  $L$  poses closest to the centroids of the corresponding clusters, which represent centers of object observation. For our experiments on indoor Replica and ScanNet datasets, we set  $L = 5$ . Then we select *best* object view based on the largest area of projection (Eq. 1):

$$\max_{P_l | l \in (1, \dots, L)} A(R(o_i, P_l)), \quad (1)$$

where  $R$  is the raycasting operator that converts an object’s point cloud  $p_i$  in the pose  $P_l$  into masks, and  $A$  is the operator that estimates the area of the object’s mask.

### 3.3 3D scene graph nodes generation

To describe each object (node)  $o_i$  we utilize a visual language model on a projected crop. Our internal experiments show that LLaVA 1.6 [48] performs best for indoor scene captioning. We call the model with a prompt *"Describe visible object in front of you, paying close attention to its spatial dimensions and visual attributes"*. We are also incorporating enhanced environmental awareness to prevent LLaVA from arbitrarily describing objects that are difficult to discern with a phrase *"The object is one we usually see in indoor scenes. Its signature must be short and sparse, describe appearance, geometry, material. Don't describe background."* To further improve output quality we extend the text instruction with several handcrafted examples.

### 3.4 3D Scene graph edges generation

When generating scene graph edges, we pursue two goals: 1) enabling LLM to answer complex user queries, and 2) compactly describing object relations in textual form.

To achieve these goals, we define scene graph edges as Euclidean distances between the centers of objects’ bounding boxes. Thus, each node is connected to all other nodes, helping to answer user queries. We exclude background objects (e.g., wall, floor, ceiling) from these connections, as their bounding box centers do not adequately represent their locations. For each pair of nodes  $o_i, o_j$ , the edge  $e_{ij}$  is defined as Eq. 2:

$$e_{ij} = \begin{cases} d(o_i, o_j), & \text{if } o_i \text{ and } o_j \notin \{\text{background classes}\}, \\ \text{None}, & \text{if } o_i \text{ or } o_j \in \{\text{background classes}\}, \end{cases} \quad (2)$$

where  $d(o_i, o_j)$  is the Euclidian distance between the bounding box centers of the object  $o_i$  and the object  $o_j$ .

### 3.5 Applying scene graph to a LLM

We propose using an LLM and scene text description to retrieve objects by their open vocabulary references. We store the scene description as a JSON file containing an objects list  $O$  and a list  $E$  of their connections. For each object  $i$ , we store its id ( $o_i^{id}$ ), caption ( $o_i^{caption}$ ), center ( $o_i^{center}$ ) and

extent ( $o_i^{extent}$ ) of its 3D bounding box. The relation between objects  $o_i$  and  $o_j$  includes  $o_i^{caption}$ ,  $o_i^{id}$ ,  $o_j^{caption}$ ,  $o_j^{id}$ , and the Euclidean distance between their bounding box centers ( $d_{ij}$ ).

Real scenes may contain many objects (e.g., over 100), potentially forming a fully connected graph and resulting in a long scene description (over 32k symbols). This can degrade LLM performance due to the long context. However, retrieving a referred object typically doesn't require the location of all objects. Therefore, we propose a *deductive* scene reasoning algorithm to find objects efficiently.

The *deductive* scene reasoning algorithm involves several consecutive LLM calls. First, the LLM uses as input a scene description with object IDs  $O^{id}$  and their caption  $O^{caption}$ , along with the user's query *query*. It selects semantically relevant object IDs *RelatedObjectsIds* for answering the question in *general* case. Then, we create a scene description with additional location and connection details, but only for the selected *RelatedObjects*. This results in a compact description focused on the objects relevant to the user's query in the *particular* scene.

For each object, we include a "relations" field in its description, listing sentences in the following template: "The  $o_i^{caption}$  with id  $o_i^{id}$  is at distance  $d_{ij}$  m from the  $o_j^{caption}$  with id  $o_j^{id}$ ". To limit scene description length, we cap the number of connections per object to  $n_{rel}^{max}$ .

Using the compact scene description of relevant objects, the LLM retrieves the final objects in JSON format. If the response needs formatting, we make another LLM call to adjust it.

Algorithm 1 details our scene *deductive* inference algorithm. Results in Section 4.2 demonstrate the benefits of incorporating spatial metric relations in the scene description and employing the *deductive* scene reasoning algorithm for object retrieval using LLM.

---

**Algorithm 1** *Deductive* scene reasoning algorithm ( $O^{id}, O^{caption}, O^{center}, O^{extent}, E, query$ )

---

```

RelatedObjectsIds ← LLM(query,  $O^{id}, O^{caption}$ )
N ← number of RelatedObjectsIds
RelatedObjects ← ∅
for i in range (0, N) do
   $o_i^{relations}$  ← ∅
  for j in range (0, N) do
    if  $E_{ij}$  exists and number of  $o_i^{relations} < n_{rel}^{max}$  then
      Append  $E_{ij}$  to  $o_i^{relations}$ 
    end if
  end for
  RelatedObject ← { $o_i^{id}, o_i^{caption}, o_i^{center}, o_i^{extent}, o_i^{relations}$ }
  Append RelatedObject to RelatedObjects
end for
FinalAnswer ← LLM(query, RelatedObjects)
FinalObjectId ← parse(FinalAnswer)
if Failed to parse FinalObjectId then
  FinalAnswer ← LLM(FinalAnswer)
  FinalObjectId ← parse(FinalAnswer)
end if

```

---

## 4 Experiments

We conduct our experiments on Replica and ScanNet RGB-D data. For each datasets we select 8 scenes: (*room0, room1, room2, office0, office1, office2, office3, office4*) and (*0011\_00, 0030\_00, 0046\_00, 0086\_00, 0222\_00, 0378\_00, 0389\_00, 0435\_00*) respectively. With the provided GT semantic segmentation annotation we perform 3D open-vocabulary benchmarking with the closest related works (Sec. 4.1) to show advantage of BBQ 3D object-centric map scene representation. To examine the ability to answer complex queries that contain object relations we utilize ScanNet annotations from Sr3D and Nr3D datasets. The Sr3D dataset contains template-based references to objects based on their spatial relations with other objects. The Nr3D dataset contains various human-annotated natural language object references. For the template-based Sr3D dataset, we select a subsample of 526 queries that represent unique triplets of (*target, relation, anchor*) for the eight considered scenes from ScanNet and similarly for the natural language Nr3D dataset, choosing those queries that only involve spatial relationships with other objects. Results are provided in Sec. 4.2. All the experiments were conducted on a single Nvidia V100 with 32 GB of vRAM except for LLM where we use Nvidia H100 with 80 GB of vRAM.

## 4.1 3D open-vocabulary semantic segmentation

To perform 3D open-vocabulary segmentation we extract CLIP features from each object *best* view. Our internal ablation between OpenCLIP Ilharco et al. [61], SigLip [5], and Eva2 [3] shows that the last model performs better in terms of quality by a large margin. We utilize Eva2 with the blur technique [69] and call this method BBQ-CLIP.

### 4.1.1 Evaluation protocol

For all methods, we query only classes that exist on each scene inside the phrase "*an image of <class\_name>*" and calculate mAcc, mIoU, and frequency-weighted mIoU.

### 4.1.2 Results

As shown in Tab. 1, our BBQ-CLIP approach shows best results among other zero-shot algorithms (ConceptFusion[22], ConceptGraph[24], OpenMask3D[31]) in the 3D open-vocabulary segmentation and almost achieve OpenFusion[25]. We position OpenFusion in a privileged group because the method exploits SEEM [18], which was trained on three supervised segmentation tasks: panoptic, referring, and interactive.

Table 1: 3D open-vocabulary semantic segmentation benchmark.

Methods		mAcc↑	Replica mIoU↑	fmIoU↑	mAcc↑	ScanNet mIoU↑	fmIoU↑
<i>Privileged</i>	OpenFusion [25]	0.41	0.30	0.58	0.67	0.53	0.64
<i>Zero-shot</i>	ConceptFusion [22]	0.29	0.11	0.14	0.49	0.26	0.31
	OpenMask3D [31]	-	-	-	0.34	0.18	0.20
	ConceptGraphs [24]	0.36	0.18	0.15	0.52	0.26	0.29
	<b>BBQ-CLIP</b>	<b>0.38</b>	<b>0.27</b>	<b>0.48</b>	<b>0.56</b>	<b>0.34</b>	<b>0.36</b>

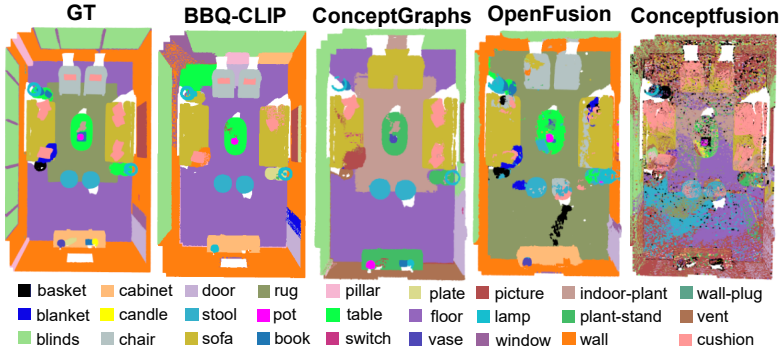


Figure 3: Qualitative examples of 3D open-vocabulary semantic segmentation on the Replica.

## 4.2 Scene graphs generation

### 4.2.1 Evaluation protocol

During ablation experiments, we assess various methods for constructing a graph from ground-truth point clouds of objects. We evaluate object retrieval quality using the *Recall@1* [24]. For experiments involving scene reconstruction, we use such metrics as *Acc@0.1* [36], *Acc@0.25* [70]. A prediction is considered true positive if the Intersection over Union (IoU) between the selected object bounding box and the ground truth bounding box exceeds 0.1 and 0.25, respectively.

## 4.2.2 Results

Table 2: Ablation study on graph edges type on Sr3D subset.

Edges type	Types of semantic relations	Recall @ 1
no edges	-	0.52
<b>GT distance</b>	-	<b>0.74</b>
GT semantic	supporting, supported-by, above, below	0.59
GT semantic and GT distance	supporting, supported-by, above, below	0.72

Table 3: Ablation study on graph edges presence in LLM prompt on Sr3D and Nr3D datasets.

LLM	Graph edges in prompt	Recall@1 Sr3D	Recall@1 Nr3D
Mistral-7B [71]	no	0.46	0.36
<b>Mistral-7B</b> [71]	<b>yes</b>	<b>0.54</b>	<b>0.41</b>
LLAMA3-8B [72]	no	0.52	0.38
<b>LLAMA3-8B</b> [72]	<b>yes</b>	<b>0.74</b>	<b>0.49</b>
Mixtral8x7b [73]	no	0.60	0.43
<b>Mixtral8x7b</b> [73]	<b>yes</b>	<b>0.71</b>	<b>0.48</b>
LLAMA3-70B [72]	no	0.78	0.51
<b>LLAMA3-70B</b> [72]	<b>yes</b>	<b>0.92</b>	<b>0.65</b>

Table 4: 3D referred object retrieval on Sr3D and Nr3D datasets.

Method	Scene Reasoning Algorithm	Edges	Acc@0.1 Sr3D	Acc@0.25 Sr3D	Acc@0.1 Nr3D	Acc@0.25 Nr3D
GT	Random	-	0.03	0.02	0.02	0.01
BBQ (ours)	Random	-	0.02	0.01	0.02	0.01
ConceptGraphs[24]	ConceptGraphs	-	0.08	0.02	0.07	0.03
ConceptGraphs[24]	<i>Deductive</i> (ours)	-	0.15	0.08	0.12	0.08
Open-Fusion [25]	CLIP	-	0.13	0.02	0.10	0.02
BBQ (ours)	CLIP	-	0.10	0.06	0.12	0.06
<b>BBQ (ours)</b>	<b><i>Deductive</i> (ours)</b>	<b>distance</b>	<b>0.23</b>	<b>0.18</b>	<b>0.19</b>	<b>0.10</b>

**Edges type.** The Sr3D dataset annotates spatial semantic relations between referred objects and those mentioned in the reference. We explore methods for integrating these relations into the text description of a scene. Ground truth semantic relations include: *supporting*, *supported by*, *above*, and *below*. These relations can be determined by object categories and 3D locations. We conduct experiments on combining metric and semantic edges. When no semantic relation exists, we add a metric edge. We use LLAMA3-8B [72] in this ablation study. We find that metric edges yield the most substantial improvement over scenes lacking graph edges, as shown in Table 2.

**Graph Edges in LLM prompt.** Adding metric edges benefits not only LLAMA3-8B but also other state-of-the-art LLMs. Table 3 illustrates that integrating graph edges into the LLM prompt significantly improves *Recall@0.1* for object retrieval across Mistral-7B [71], LLAMA3-8B [72], Mixtral-8x7B [73], and LLAMA3-70B [72] on the Sr3D dataset. This improvement extends to the Nr3D dataset containing more challenging natural language queries for object retrieval.

**BBQ performance comparison with different approaches.** Our approach surpasses existing open-vocabulary methods for 3D object retrieval, notably outperforming ConceptGraphs [24], which also integrates an LLM with scene text descriptions (Table 4). In these experiments, we use the open LLAMA3-8B model [72] for all methods. One of the key contributions comes from our *deductive* scene reasoning algorithm. By applying it to ConceptGraphs’ scene description, we nearly double the accuracy metrics by reducing the length of the LLM prompt in a single inference call. Moreover, we demonstrate that leveraging an object-centric textual description of a scene graph,

interfaced via an LLM, significantly outperforms methods utilizing CLIP features for object retrieval, such as OpenFusion [25] and our BBQ method interfaced with CLIP text embeddings of object queries. Additionally, we conduct experiments with a random object retrieval strategy to highlight the challenge of solving this task in zero-shot mode.

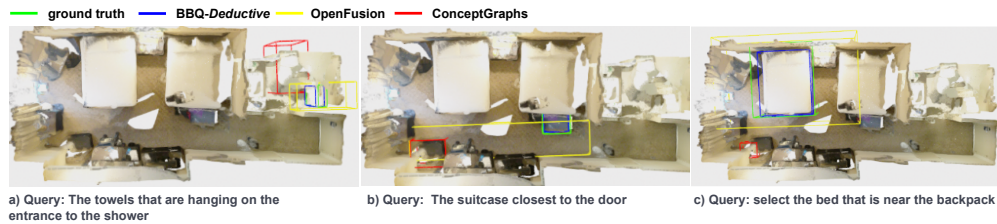


Figure 4: Qualitative examples of 3D referred object retrieval on the Sr3D/Nr3D datasets.

### 4.3 Time consumption analysis

We perform time consumption analysis on a machine with *Intel(R) Xeon(R) Gold 6154 CPU @ 3.00GHz* and *Tesla V100-SXM2-32GB*. On Replica scenes with a mean of 30 detections per frame and 100 average number of objects, our pipeline runs with 1-1.5 fps per second for 3D object-centric map construction. In contrast, our closest analog ConceptGraphs [24] requires 4-5 seconds to perform the same task. We achieve such fast results due to MobileSAMv2[52] (0.2s per frame), DINO embeddings (0.12s per frame), GPU realization of DBSCAN noise removal (mean 0.005s per object), IOU-based spatial similarities, and GPU-based clusterization to drastically reduce *best* view search space for 3D to 2D raycasting projection.

## 5 Limitations

Conducted experiments highlight that our 3D object-centric map construction method is limited in its ability to successfully distinguish tiny objects in the image. This happens because such areas are usually indicated as low-confidence proposals and discarded in the filtering stage or the visual DINO descriptor is not distinguish enough from the background due to the patch size extraction technique. Thus, BBQ requires more scene exploration where the camera will be placed closer to objects of interest to successfully map such instances.

## 6 Conclusion

We propose a novel modular BBQ approach that relies entirely on underlying foundation models and transcends the basic requirements of a 3D object retrieval problem. With BBQ, we advance the limits of 3D scene perception by integrating language models with general world knowledge and our scene-specific graph representation. The successful outcomes of our experiments on the complex Nr3D and Sr3D datasets demonstrate the effectiveness of our approach, opening new avenues for a more comprehensive and flexible understanding and interaction with 3D scenes. We hope that our time-efficient efforts will facilitate BBQ applications in real-world robotics projects that bridge the communication gap between humans and autonomous agents.

## References

- [1] Alec Radford, Jong Wook Kim, Chris Hallacy, Aditya Ramesh, Gabriel Goh, Sandhini Agarwal, Girish Sastry, Amanda Askell, Pamela Mishkin, Jack Clark, et al. Learning transferable visual models from natural language supervision. In *International conference on machine learning*, pages 8748–8763. PMLR, 2021.
- [2] Norman Mu, Alexander Kirillov, David Wagner, and Saining Xie. Slip: Self-supervision meets language-image pre-training. In *European conference on computer vision*, pages 529–544. Springer, 2022.

- [3] Yuxin Fang, Quan Sun, Xinggang Wang, Tiejun Huang, Xinlong Wang, and Yue Cao. Eva-02: A visual representation for neon genesis. *arXiv preprint arXiv:2303.11331*, 2023.
- [4] Quan Sun, Jinsheng Wang, Qiyang Yu, Yufeng Cui, Fan Zhang, Xiaosong Zhang, and Xinlong Wang. Eva-clip-18b: Scaling clip to 18 billion parameters. *arXiv preprint arXiv:2402.04252*, 2024.
- [5] Xiaohua Zhai, Basil Mustafa, Alexander Kolesnikov, and Lucas Beyer. Sigmoid loss for language image pre-training. In *Proceedings of the IEEE/CVF International Conference on Computer Vision*, pages 11975–11986, 2023.
- [6] Rohit Girdhar, Alaaeldin El-Nouby, Zhuang Liu, Mannat Singh, Kalyan Vasudev Alwala, Armand Joulin, and Ishan Misra. Imagebind: One embedding space to bind them all. In *Proceedings of the IEEE/CVF Conference on Computer Vision and Pattern Recognition*, pages 15180–15190, 2023.
- [7] Xiuye Gu, Tsung-Yi Lin, Weicheng Kuo, and Yin Cui. Open-vocabulary object detection via vision and language knowledge distillation. *arXiv preprint arXiv:2104.13921*, 2021.
- [8] Yiwu Zhong, Jianwei Yang, Pengchuan Zhang, Chunyuan Li, Noel Codella, Liunian Harold Li, Luwei Zhou, Xiyang Dai, Lu Yuan, Yin Li, et al. Regionclip: Region-based language-image pretraining. In *Proceedings of the IEEE/CVF Conference on Computer Vision and Pattern Recognition*, pages 16793–16803, 2022.
- [9] Boyi Li, Kilian Q Weinberger, Serge Belongie, Vladlen Koltun, and René Ranftl. Language-driven semantic segmentation. *arXiv preprint arXiv:2201.03546*, 2022.
- [10] Zheng Ding, Jieke Wang, and Zhuowen Tu. Open-vocabulary universal image segmentation with maskclip. *arXiv preprint arXiv:2208.08984*, 2022.
- [11] Golnaz Ghiasi, Xiuye Gu, Yin Cui, and Tsung-Yi Lin. Scaling open-vocabulary image segmentation with image-level labels. In *European Conference on Computer Vision*, pages 540–557. Springer, 2022.
- [12] Seokju Cho, Heeseong Shin, Sunghwan Hong, Seungjun An, Seungjun Lee, Anurag Arnab, Paul Hongsuck Seo, and Seungryong Kim. Cat-seg: Cost aggregation for open-vocabulary semantic segmentation. *arXiv preprint arXiv:2303.11797*, 2023.
- [13] Feng Liang, Bichen Wu, Xiaoliang Dai, Kunpeng Li, Yinan Zhao, Hang Zhang, Peizhao Zhang, Peter Vajda, and Diana Marculescu. Open-vocabulary semantic segmentation with mask-adapted clip. In *Proceedings of the IEEE/CVF Conference on Computer Vision and Pattern Recognition*, pages 7061–7070, 2023.
- [14] Zeyi Sun, Ye Fang, Tong Wu, Pan Zhang, Yuhang Zang, Shu Kong, Yuanjun Xiong, Dahua Lin, and Jiaqi Wang. Alpha-clip: A clip model focusing on wherever you want. *arXiv preprint arXiv:2312.03818*, 2023.
- [15] Hao Zhang, Feng Li, Xueyan Zou, Shilong Liu, Chunyuan Li, Jianwei Yang, and Lei Zhang. A simple framework for open-vocabulary segmentation and detection. In *Proceedings of the IEEE/CVF International Conference on Computer Vision*, pages 1020–1031, 2023.
- [16] Xueyan Zou, Zi-Yi Dou, Jianwei Yang, Zhe Gan, Linjie Li, Chunyuan Li, Xiyang Dai, Harkirat Behl, Jianfeng Wang, Lu Yuan, et al. Generalized decoding for pixel, image, and language. In *Proceedings of the IEEE/CVF Conference on Computer Vision and Pattern Recognition*, pages 15116–15127, 2023.
- [17] Jiarui Xu, Sifei Liu, Arash Vahdat, Wonmin Byeon, Xiaolong Wang, and Shalini De Mello. Open-vocabulary panoptic segmentation with text-to-image diffusion models. In *Proceedings of the IEEE/CVF Conference on Computer Vision and Pattern Recognition*, pages 2955–2966, 2023.
- [18] Xueyan Zou, Jianwei Yang, Hao Zhang, Feng Li, Linjie Li, Jianfeng Wang, Lijuan Wang, Jianfeng Gao, and Yong Jae Lee. Segment everything everywhere all at once. *Advances in Neural Information Processing Systems*, 36, 2024.
- [19] Mike Ranzinger, Greg Heinrich, Jan Kautz, and Pavlo Molchanov. Am-radio: Agglomerative model—reduce all domains into one. *arXiv preprint arXiv:2312.06709*, 2023.
- [20] Nikolaos Tsagkas, Oisín Mac Aodha, and Chris Xiaoxuan Lu. V1-fields: Towards language-grounded neural implicit spatial representations. *arXiv preprint arXiv:2305.12427*, 2023.
- [21] Huy Ha and Shuran Song. Semantic abstraction: Open-world 3d scene understanding from 2d vision-language models. *arXiv preprint arXiv:2207.11514*, 2022.

- [22] Krishna Murthy Jatavallabhula, Alihusein Kuwajerwala, Qiao Gu, Mohd Omama, Tao Chen, Shuang Li, Ganesh Iyer, Soroush Saryazdi, Nikhil Keetha, Ayush Tewari, Joshua B. Tenenbaum, Celso Miguel de Melo, Madhava Krishna, Liam Paull, Florian Shkurti, and Antonio Torralba. Conceptfusion: Open-set multimodal 3d mapping. *Robotics: Science and Systems (RSS)*, 2023.
- [23] Shiyang Lu, Haonan Chang, Eric Pu Jing, Abdeslam Boularias, and Kostas Bekris. Ovir-3d: Open-vocabulary 3d instance retrieval without training on 3d data. In *Conference on Robot Learning*, pages 1610–1620. PMLR, 2023.
- [24] Qiao Gu, Alihusein Kuwajerwala, Sacha Morin, Krishna Murthy Jatavallabhula, Bipasha Sen, Aditya Agarwal, Corban Rivera, William Paul, Kirsty Ellis, Rama Chellappa, et al. Conceptgraphs: Open-vocabulary 3d scene graphs for perception and planning. In *2024 IEEE International Conference on Robotics and Automation (ICRA)*, 2024.
- [25] Kashu Yamazaki, Taisei Hanyu, Khoa Vo, Thang Pham, Minh Tran, Gianfranco Doretto, Anh Nguyen, and Ngan Le. Open-fusion: Real-time open-vocabulary 3d mapping and queryable scene representation. *arXiv preprint arXiv:2310.03923*, 2023.
- [26] Yining Hong, Haoyu Zhen, Peihao Chen, Shuhong Zheng, Yilun Du, Zhenfang Chen, and Chuang Gan. 3d-llm: Injecting the 3d world into large language models. *Advances in Neural Information Processing Systems*, 36:20482–20494, 2023.
- [27] Zhening Huang, Xiaoyang Wu, Xi Chen, Hengshuang Zhao, Lei Zhu, and Joan Lasenby. Openins3d: Snap and lookup for 3d open-vocabulary instance segmentation. *arXiv preprint arXiv:2309.00616*, 2023.
- [28] Haifeng Huang, Zehan Wang, Rongjie Huang, Luping Liu, Xize Cheng, Yang Zhao, Tao Jin, and Zhou Zhao. Chat-3d v2: Bridging 3d scene and large language models with object identifiers. *arXiv preprint arXiv:2312.08168*, 2023.
- [29] Phuc DA Nguyen, Tuan Duc Ngo, Chuang Gan, Evangelos Kalogerakis, Anh Tran, Cuong Pham, and Khoi Nguyen. Open3dis: Open-vocabulary 3d instance segmentation with 2d mask guidance. *arXiv preprint arXiv:2312.10671*, 2023.
- [30] Jihan Yang, Runyu Ding, Weipeng Deng, Zhe Wang, and Xiaojuan Qi. Regionplc: Regional point-language contrastive learning for open-world 3d scene understanding. *arXiv preprint arXiv:2304.00962*, 2023.
- [31] Ayça Takmaz, Elisabetta Fedele, Robert W Sumner, Marc Pollefeys, Federico Tombari, and Francis Engelmann. Openmask3d: Open-vocabulary 3d instance segmentation. *arXiv preprint arXiv:2306.13631*, 2023.
- [32] Songyou Peng, Kyle Genova, Chiyu Jiang, Andrea Tagliasacchi, Marc Pollefeys, Thomas Funkhouser, et al. Openscene: 3d scene understanding with open vocabularies. In *Proceedings of the IEEE/CVF Conference on Computer Vision and Pattern Recognition*, pages 815–824, 2023.
- [33] Sebastian Koch, Narunas Vaskevicius, Mirco Colosi, Pedro Hermosilla, and Timo Ropinski. Open3dsg: Open-vocabulary 3d scene graphs from point clouds with queryable objects and open-set relationships. *arXiv preprint arXiv:2402.12259*, 2024.
- [34] Rao Fu, Jingyu Liu, Xilun Chen, Yixin Nie, and Wenhan Xiong. Scene-llm: Extending language model for 3d visual understanding and reasoning. *arXiv preprint arXiv:2403.11401*, 2024.
- [35] Yingda Yin, Yuzheng Liu, Yang Xiao, Daniel Cohen-Or, Jingwei Huang, and Baoquan Chen. Sai3d: Segment any instance in 3d scenes. *arXiv preprint arXiv:2312.11557*, 2023.
- [36] Abdelrhman Werby, Chenguang Huang, Martin Büchner, Abhinav Valada, and Wolfram Burgard. Hierarchical open-vocabulary 3d scene graphs for language-grounded robot navigation. In *First Workshop on Vision-Language Models for Navigation and Manipulation at ICRA 2024*, 2024.
- [37] Justin Kerr, Chung Min Kim, Ken Goldberg, Angjoo Kanazawa, and Matthew Tancik. Lurf: Language embedded radiance fields. In *Proceedings of the IEEE/CVF International Conference on Computer Vision*, pages 19729–19739, 2023.
- [38] Kunhao Liu, Fangneng Zhan, Jiahui Zhang, Muyu Xu, Yingchen Yu, Abdulmotaleb El Saddik, Christian Theobalt, Eric Xing, and Shijian Lu. Weakly supervised 3d open-vocabulary segmentation. *Advances in Neural Information Processing Systems*, 36:53433–53456, 2023.
- [39] Guibiao Liao, Kaichen Zhou, Zhenyu Bao, Kanglin Liu, and Qing Li. Ov-nerf: Open-vocabulary neural radiance fields with vision and language foundation models for 3d semantic understanding. *arXiv preprint arXiv:2402.04648*, 2024.

- [40] Muer Tie, Julong Wei, Zhengjun Wang, Ke Wu, Shansuai Yuan, Kaizhao Zhang, Jie Jia, Jieru Zhao, Zhongxue Gan, and Wenchao Ding. O2v-mapping: Online open-vocabulary mapping with neural implicit representation. *arXiv preprint arXiv:2404.06836*, 2024.
- [41] Haiyang Ying, Yixuan Yin, Jinzhi Zhang, Fan Wang, Tao Yu, Ruqi Huang, and Lu Fang. Omnise3d: Omniversal 3d segmentation via hierarchical contrastive learning. *arXiv preprint arXiv:2311.11666*, 2023.
- [42] Jin-Chuan Shi, Miao Wang, Hao-Bin Duan, and Shao-Hua Guan. Language embedded 3d gaussians for open-vocabulary scene understanding. *arXiv preprint arXiv:2311.18482*, 2023.
- [43] Minghan Qin, Wanhua Li, Jiawei Zhou, Haoqian Wang, and Hanspeter Pfister. Langsplat: 3d language gaussian splatting. *arXiv preprint arXiv:2312.16084*, 2023.
- [44] Sicheng Jiang. *Feature 3DGS: Supercharging 3D Gaussian Splatting to Enable Distilled Feature Fields*. University of California, Los Angeles, 2023.
- [45] Maria Tsimpoukelli, Jacob L Menick, Serkan Cabi, SM Eslami, Oriol Vinyals, and Felix Hill. Multimodal few-shot learning with frozen language models. *Advances in Neural Information Processing Systems*, 34: 200–212, 2021.
- [46] Junnan Li, Dongxu Li, Silvio Savarese, and Steven Hoi. Blip-2: Bootstrapping language-image pre-training with frozen image encoders and large language models. In *International conference on machine learning*, pages 19730–19742. PMLR, 2023.
- [47] Haotian Liu, Chunyuan Li, Qingyang Wu, and Yong Jae Lee. Visual instruction tuning, 2023.
- [48] Haotian Liu, Chunyuan Li, Yuheng Li, and Yong Jae Lee. Improved baselines with visual instruction tuning, 2023.
- [49] Haotian Liu, Chunyuan Li, Yuheng Li, Bo Li, Yuanhan Zhang, Sheng Shen, and Yong Jae Lee. Llava-next: Improved reasoning, ocr, and world knowledge. January 2024. URL <https://llava-v1.github.io/blog/2024-01-30-llava-next/>.
- [50] Kibum Kim, Kanghoon Yoon, Jaehyeong Jeon, Yeonjun In, Jinyoung Moon, Donghyun Kim, and Chanyoung Park. Llm4sgg: Large language model for weakly supervised scene graph generation. *arXiv e-prints*, pages arXiv–2310, 2023.
- [51] Alexander Kirillov, Eric Mintun, Nikhila Ravi, Hanzi Mao, Chloe Rolland, Laura Gustafson, Tete Xiao, Spencer Whitehead, Alexander C Berg, Wan-Yen Lo, et al. Segment anything. In *Proceedings of the IEEE/CVF International Conference on Computer Vision*, pages 4015–4026, 2023.
- [52] Chaoning Zhang, Dongshen Han, Sheng Zheng, Jinwoo Choi, Tae-Ho Kim, and Choong Seon Hong. Mobilesamv2: Faster segment anything to everything. *arXiv preprint arXiv:2312.09579*, 2023.
- [53] Jonas Schult, Francis Engelmann, Alexander Hermans, Or Litany, Siyu Tang, and Bastian Leibe. Mask3d: Mask transformer for 3d semantic instance segmentation. In *2023 IEEE International Conference on Robotics and Automation (ICRA)*, pages 8216–8223. IEEE, 2023.
- [54] Haoyu Guo, He Zhu, Sida Peng, Yuang Wang, Yujun Shen, Ruizhen Hu, and Xiaowei Zhou. Sam-guided graph cut for 3d instance segmentation. *arXiv preprint arXiv:2312.08372*, 2023.
- [55] Mohamed El Banani, Amit Raj, Kevis-Kokitsi Maninis, Abhishek Kar, Yuanzhen Li, Michael Rubinstein, Deqing Sun, Leonidas Guibas, Justin Johnson, and Varun Jampani. Probing the 3d awareness of visual foundation models. *arXiv preprint arXiv:2404.08636*, 2024.
- [56] Shun-Cheng Wu, Keisuke Tateno, Nassir Navab, and Federico Tombari. Incremental 3d semantic scene graph prediction from rgb sequences. In *Proceedings of the IEEE/CVF Conference on Computer Vision and Pattern Recognition*, pages 5064–5074, 2023.
- [57] Ziqin Wang, Bowen Cheng, Lichen Zhao, Dong Xu, Yang Tang, and Lu Sheng. Vl-sat: visual-linguistic semantics assisted training for 3d semantic scene graph prediction in point cloud. In *Proceedings of the IEEE/CVF Conference on Computer Vision and Pattern Recognition*, pages 21560–21569, 2023.
- [58] Yiding Qiu and Henrik I Christensen. 3d scene graph prediction on point clouds using knowledge graphs. In *2023 IEEE 19th International Conference on Automation Science and Engineering (CASE)*, pages 1–7. IEEE, 2023.
- [59] Sebastian Koch, Pedro Hermosilla, Narunas Vaskevicius, Mirco Colosi, and Timo Ropinski. Sgrec3d: Self-supervised 3d scene graph learning via object-level scene reconstruction. In *Proceedings of the IEEE/CVF Winter Conference on Applications of Computer Vision*, pages 3404–3414, 2024.

- [60] Zhu Ziyu, Ma Xiaojian, Chen Yixin, Deng Zhidong, Huang Siyuan, and Li Qing. 3d-vista: Pre-trained transformer for 3d vision and text alignment. In *ICCV*, 2023.
- [61] Gabriel Ilharco, Mitchell Wortsman, Ross Wightman, Cade Gordon, Nicholas Carlini, Rohan Taori, Achal Dave, Vaishal Shankar, Hongseok Namkoong, John Miller, Hannaneh Hajishirzi, Ali Farhadi, and Ludwig Schmidt. Openclip, July 2021. URL <https://doi.org/10.5281/zenodo.5143773>. If you use this software, please cite it as below.
- [62] Mathilde Caron, Hugo Touvron, Ishan Misra, Hervé Jégou, Julien Mairal, Piotr Bojanowski, and Armand Joulin. Emerging properties in self-supervised vision transformers. In *Proceedings of the IEEE/CVF international conference on computer vision*, pages 9650–9660, 2021.
- [63] Maxime Oquab, Timothée Darcet, Théo Moutakanni, Huy Vo, Marc Szafraniec, Vasil Khalidov, Pierre Fernandez, Daniel Haziza, Francisco Massa, Alaaeldin El-Nouby, et al. Dinov2: Learning robust visual features without supervision. *arXiv preprint arXiv:2304.07193*, 2023.
- [64] Narek Tumanyan, Assaf Singer, Shai Bagon, and Tali Dekel. Dino-tracker: Taming dino for self-supervised point tracking in a single video. *arXiv preprint arXiv:2403.14548*, 2024.
- [65] Shir Amir, Yossi Gandelsman, Shai Bagon, and Tali Dekel. Deep vit features as dense visual descriptors. *arXiv preprint arXiv:2112.05814*, 2(3):4, 2021.
- [66] Nikhil Keetha, Avneesh Mishra, Jay Karhade, Krishna Murthy Jatavallabhula, Sebastian Scherer, Madhava Krishna, and Sourav Garg. Anyloc: Towards universal visual place recognition. *IEEE Robotics and Automation Letters*, 2023.
- [67] Panos Achlioptas, Ahmed Abdelreheem, Fei Xia, Mohamed Elhoseiny, and Leonidas J. Guibas. ReferIt3D: Neural listeners for fine-grained 3d object identification in real-world scenes. In *16th European Conference on Computer Vision (ECCV)*, 2020.
- [68] Timothée Darcet, Maxime Oquab, Julien Mairal, and Piotr Bojanowski. Vision transformers need registers. *arXiv preprint arXiv:2309.16588*, 2023.
- [69] Lingfeng Yang, Yueze Wang, Xiang Li, Xinlong Wang, and Jian Yang. Fine-grained visual prompting. *Advances in Neural Information Processing Systems*, 36, 2024.
- [70] Dave Zhenyu Chen, Angel X Chang, and Matthias Nießner. Scanrefer: 3d object localization in rgb-d scans using natural language. In *European conference on computer vision*, pages 202–221. Springer, 2020.
- [71] Albert Q Jiang, Alexandre Sablayrolles, Arthur Mensch, Chris Bamford, Devendra Singh Chaplot, Diego de las Casas, Florian Bressand, Gianna Lengyel, Guillaume Lample, Lucile Saulnier, et al. Mistral 7b. *arXiv preprint arXiv:2310.06825*, 2023.
- [72] AI@Meta. Llama 3 model card. 2024. URL [https://github.com/meta-llama/llama3/blob/main/MODEL\\_CARD.md](https://github.com/meta-llama/llama3/blob/main/MODEL_CARD.md).
- [73] Albert Q Jiang, Alexandre Sablayrolles, Antoine Roux, Arthur Mensch, Blanche Savary, Chris Bamford, Devendra Singh Chaplot, Diego de las Casas, Emma Bou Hanna, Florian Bressand, et al. Mixtral of experts. *arXiv preprint arXiv:2401.04088*, 2024.
- [74] Alexander Kirillov, Eric Mintun, Nikhila Ravi, Hanzi Mao, Chloe Rolland, Laura Gustafson, Tete Xiao, Spencer Whitehead, Alexander C. Berg, Wan-Yen Lo, Piotr Dollár, and Ross Girshick. Segment anything. *arXiv:2304.02643*, 2023.
- [75] Haoxuan You, Haotian Zhang, Zhe Gan, Xianzhi Du, Bowen Zhang, Zirui Wang, Liangliang Cao, Shih-Fu Chang, and Yinfei Yang. Ferret: Refer and ground anything anywhere at any granularity. *arXiv preprint arXiv:2310.07704*, 2023.
- [76] Shaohan Huang, Li Dong, Wenhui Wang, Yaru Hao, Saksham Singhal, Shuming Ma, Tengchao Lv, Lei Cui, Owais Khan Mohammed, Barun Patra, et al. Language is not all you need: Aligning perception with language models. *Advances in Neural Information Processing Systems*, 36, 2024.

## A Selecting type of DINO model for visual descriptors

We choose the smallest architecture (ViT-S) and make our selection based on a trade-off between the size of pixels in the patch to preserve small objects on scenes and inference speed. To achieve this we change the stride of the patch’s convolution to 4 and 7 accordingly and interpolate positional encoding. For transformers, we only consider their training resolutions. All measurements are done on Tesla V100-SXM2-32GB with torch2.3 and cuda11.8. For DINOv2 xFormers is turned on.

Table 5: Comparison between the DINO models.

Model	Version (Num. parameters)	Patch size	Resolution, px (Num. patches)	Mean time, s (after 5 warmups)
DINO[62]	ViT-S (21M)	8	224x395 (28x49)	0.02
		4	224x395 (55x97)	0.13
DINOv2[63]	ViT-S (21M)	14	448x798 (32x57)	0.02
			224x406 (16x29)	0.01
		7	448x798 (63x113)	0.12
			224x406 (31x57)	0.02

## B Selecting type of DINO facet for visual descriptors

Several types of facets can be used for visual descriptors from the DINO transformer: *key*, *query*, *value*, and *token*. It is an open question of which facet to use. Based on their ablations, Amir et al. [65] for co-segmentation task find *key* to be most suitable, Keetha et al. [66] for a task of place recognition choose *values*, Tumanyan et al. [64] for a point tracking select *tokens*. In common authors agree that peak performance is achieved through deeper layers, somewhere between the middle and the last layer of transformers. Thus we perform a quality study (Fig. 5, Fig. 6) and in alignment with Tumanyan et al. [64] choose *value* facet that has the sharpest contrast in the similarity map to other objects, which is crucial for robust DINO-based association.

## C Ablation on 3D object-centric map construction

Table 6: Comparison between the DINO models and SAM models

Model DINO	Model SAM	Recall@0.1↑	Recall@0.25↑	Recall@0.5↑	Recall@0.75↑
DINO[62]	SAM[74]	<b>0.47</b>	0.29	0.06	0.00
	MobileSAMv2[52]	0.46	<b>0.30</b>	0.07	<b>0.01</b>
DINOv2[63]	SAM[74]	0.44	<b>0.30</b>	0.07	<b>0.01</b>
	MobileSAMv2[52]	0.44	0.25	<b>0.08</b>	0.00

## D Ablation on CLIP-based encoders

Table 7: Comparison between the CLIP models

Model CLIP	Visual prompt	mAcc↑	mIoU↑	FWmIoU↑
OpenClip ViT-H-14[61]	crop	0.34	0.20	0.23
	blackout	0.28	0.17	0.23
	blur	0.31	0.18	0.23
SigLip[5]	blur	0.34	0.18	0.20
Eva02[3]	blur	<b>0.38</b>	<b>0.27</b>	<b>0.48</b>

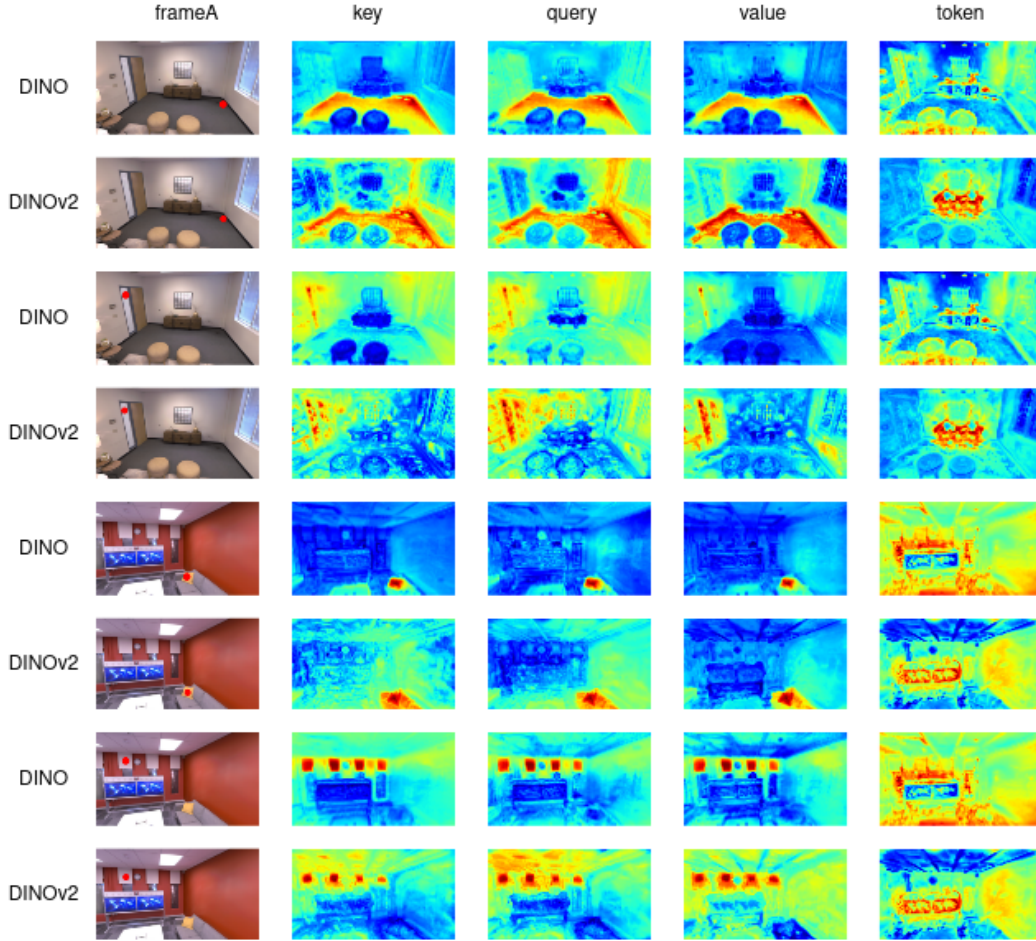


Figure 5: Qualitative ablation comparing the similarity maps of features from DINO ViT-S (stride 4, 224px) and DINOv2 (stride 7, 448px) ViT-S last (11) layer facets on the Replica dataset. On the left is an image with a query point, in the middle is a maps of the cosine similarity of the point descriptor to all descriptors from the adjacent image frame. Each map is self-scaled from 0 to 1.

## E Selecting visual language model for an image (node) captioning

Table 8: Comparison of metrics across image-captioning vLLMs

Metric	Ferret[75]	LLaVA[47]	Kosmos[76]	InternLM-2 Versions				
				VL 1.8B	7B	7B-4bit	VL 7B	VL 7B-4bit
EM@1	0.00	0.00	0.00	0.00	0.00	<b>0.03</b>	0.00	0.00
BLEU-1	0.13	<b>0.68</b>	0.23	0.56	0.61	0.59	0.37	0.44
BLEU-2	0.08	<b>0.57</b>	0.18	0.44	0.51	0.49	0.19	0.29
BLEU-3	0.06	<b>0.51</b>	0.18	0.42	0.50	0.47	0.17	0.27
BLEU-4	0.03	0.40	0.14	0.36	<b>0.46</b>	0.44	0.12	0.24
ROUGE	0.26	<b>0.77</b>	0.35	0.68	0.74	0.71	0.42	0.51
METEOR	0.31	<b>0.67</b>	0.28	0.51	0.62	0.60	0.28	0.38
HAR	0.06	<b>0.94</b>	0.33	0.69	0.81	0.75	0.72	0.64
AVG_TIME	2.61sec	0.72sec	-	<b>0.41sec</b>	0.63sec	0.58sec	0.93sec	0.71sec

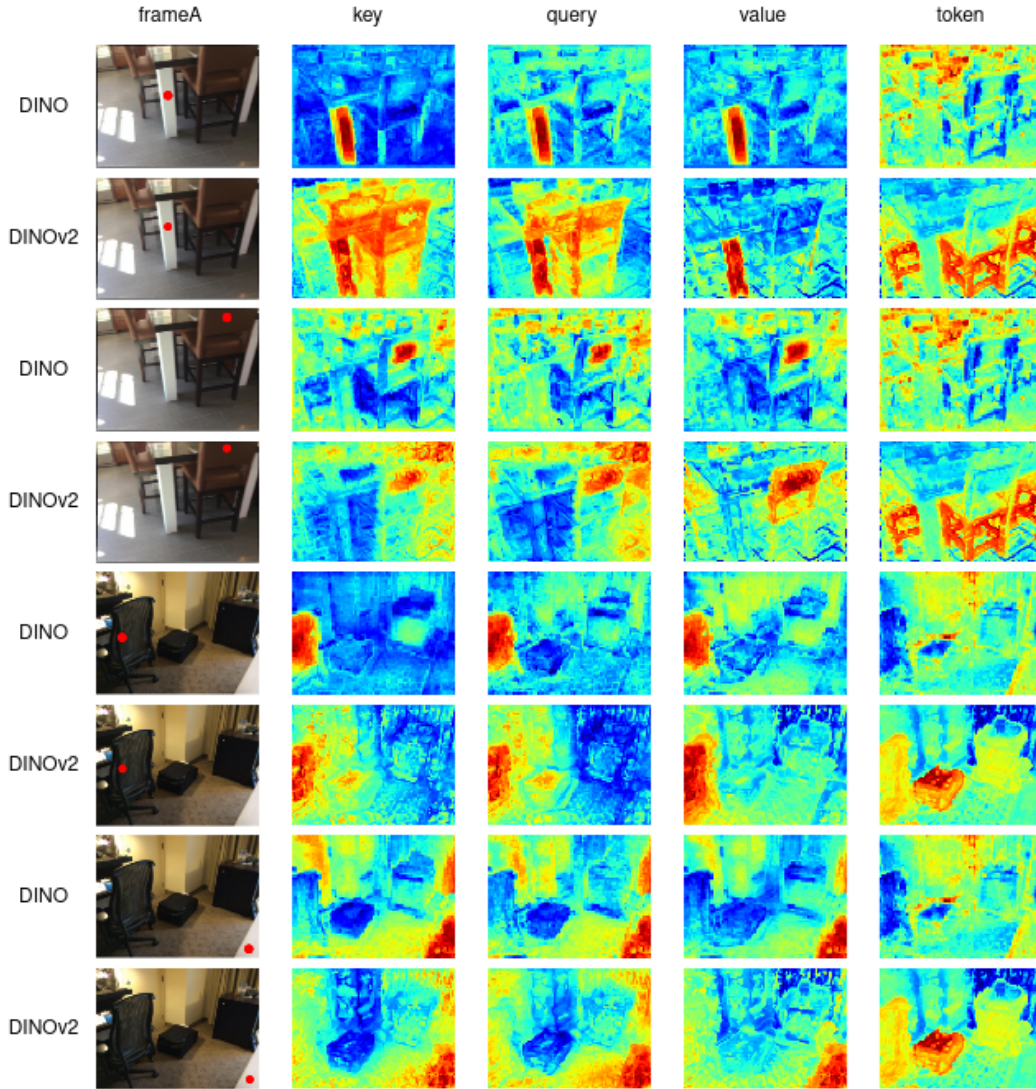


Figure 6: Qualitative ablation comparing the similarity maps of features from DINO ViT-S (stride 4, 224px, fp32) and DINOv2 (stride 7, 448px, fp32) ViT-S last (11) layer facets on the ScanNet dataset. On the left is an image with a query point, in the middle is a maps of the cosine similarity of the point descriptor to all descriptors from the adjacent image frame. Each map is self-scaled from 0 to 1.

We present the results of a benchmark analysis to determine which model best follows the defined answer format: *"The {object} is {color} and made of {material}."* The dataset for this benchmark is manually created from scene\_00 of the ScanRefer dataset, where 36 object images are carefully extracted, and captions are manually created to ensure relevance and uniformity. This manual preparation is crucial for maintaining a standardized answer format across various requests.

The Human Acceptance Rate (HAR) is one of the metrics used to evaluate each model based on its ability to produce relevant and format-adhering answers. LLaVA performs outstandingly in this regard, achieving the highest HAR of 0.9444, which signifies that nearly 94.44% of its responses are judged satisfactory. This model consistently delivers highly relevant answers, aligning closely with the required answer pattern, and thus provides the best performance among all evaluated models.

On the other end of the spectrum, Ferret has the lowest HAR at just 0.0556. This result is primarily due to the model's tendency to generate overly lengthy descriptions filled with unnecessary details, which often diverged significantly from the desired format.

Kosmos exhibits difficulties in correctly identifying objects, which significantly affects its performance, resulting in a HAR of 0.3333. This misunderstanding of objects led to answers that frequently deviated from the specified format.

The InternLM VL 1.8B model also faces challenges related to object recognition, particularly when dealing with smaller objects, which likely contributed to its middling HAR of 0.6944. This issue underscores the model's limitations in accurately processing and interpreting key details within inputs.

Comparing the InternLM versions, it was observed that models prefixed with "VL" tend to produce longer and more detailed responses than their non-VL counterparts. In this benchmark, such verbosity was deemed detrimental, as the benchmark criteria emphasized brevity and adherence to a specific answer structure. As a result, even though models like InternLM 7B and InternLM 7B-4bit have respectable HAR scores of 0.8056 and 0.7500, respectively, the "VL" models generally underperformed in this context due to their propensity for elaboration, as evidenced by the HAR scores of InternLM VL 7B and InternLM VL 7B-4bit at 0.7222 and 0.6389, respectively.

In summary, the benchmark reveals significant differences in model performances concerning format adherence and relevancy of answers, with LLaVA emerging as the most suitable model for generating consistent and format-compliant responses, while others struggle with issues ranging from verbosity to object misidentification.

## F LLaVA prompt

To describe object we call LLaVA1.6 with projected 2D crop (30 px padding) and text prompt:

*Describe visible object in front of you, paying close attention to its spatial dimensions and visual attributes. The object is one we usually see in indoor scenes. Its signature must be short and sparse, describe appearance, geometry, material. Don't describe background. Fit your description in four or five words. Examples: a closed wooden door with a glass panel; a pillow with a floral pattern; a wooden table; a gray wall..*

## G LLM prompt

Example of LLM prompts and answers while executing the *deductive* scene reasoning algorithm. The user is referencing to "the table that is close to the armchair".

**USER:**

I will describe a 3D scene using a list of objects placed in the scene. Each object is described by its semantic type and its object id. I will ask you questions about this scene.

The list of objects in the scene is the following. the floor with id 0, the kitchen cabinet with id 1, the table with id 2, the armchair with id 3, the chair with id 4, the chair with id 5, the chair with id 6, the chair with id 7, the chair with id 8, the chair with id 9, the chair with id 10, the chair with id 11, the chair with id 12, the chair with id 13, the wall with id 14, the trash can with id 15, the wall with id 16, the table with id 17, the tv with id 18, the refrigerator with id 19, the cabinet with id 20, the wall with id 21, the ceiling with id 22, the window with id 23, the window with id 24, the kitchen counter with id 25, the sink with id 26, the refrigerator with id 27, the cabinet with id 28, the wall with id 29, the door with id 30, the doorframe with id 31, the trash can with id 32. Select all objects need to know to answer the user query. If there are several objects of the same semantic type, choose all of them. The query: the table that is

close to the armchair.

**LLAMA3-8B:**

To answer the query, I need to know the following objects:

- \* The armchair with id 3
- \* The table with id 2
- \* The table with id 17

These objects are necessary to determine which table is close to the armchair.

**USER:**

I will describe a 3D scene described in a JSON format. The JSON describes objects with the following three fields:

1. "id": a unique object id
2. "bbox\_center": centroid of the 3D bounding box for the object
3. "bbox\_extent": extents of the 3D bounding box for the object
4. "object\_tag": a brief (but sometimes inaccurate) tag categorizing the object
5. "relations": a list of strings (may be empty) describing spatial relations between this object and other objects in the scene. It contains types of relations and pre-computed Euclidean distances between objects.

The JSON describing the relevant objects in the scene: [{ 'id': 2, 'bbox\_center': [-0.419, 0.188, 0.429], 'bbox\_extent': [1.192, 3.638, 0.858], 'object\_tag': 'table', 'relations': ['The table with id 2 is at distance 3.47m from the armchair with ids 3.']}], { 'id': 3, 'bbox\_center': [-3.29, 2.138, 0.401], 'bbox\_extent': [0.339, 0.842, 0.801], 'object\_tag': 'armchair', 'relations': ['The armchair with id 3 is at distance 3.47 m from the table with ids 2.', 'The armchair with id 3 is at distance 5.83 m from the table with ids 17.']}], { 'id': 17, 'bbox\_center': [-0.45, -2.954, 0.441], 'bbox\_extent': [1.669, 0.409, 0.845], 'object\_tag': 'table', 'relations': ['The table with id 17 is at distance 5.83 m from the armchair with ids 3.']}], Select objects that correspond the best to the query. Deduce spatial relations between objects, using 'relations' field of JSON. The query: the table that is close to the armchair. Give me the id of selected object. Then explain me why you choose this object.

Use the following format for the answer:

```
{
  "explanation": your explanation,
  "id": id of the selected object
}
```

**LLAMA3-8B:**

```
{
  "explanation": "The object that corresponds best to the query is the table with id 2, because it is the closest table to the armchair. The query asks for the table that is close to the armchair, and the relations field in the JSON data shows that the
```

```

    table with id 2 is at a distance of 3.47 m from the armchair with
    id 3, which is the closest distance among all tables.",
    "id": 2
  }<

```

## H Results of 3D referred object retrieval on Sr3D and Nr3D datasets

ConceptGraphs give an answer to the query of "the towels that are hanging on the entrance to the shower", which is shown in the figure 7 with a red bounding box, giving the following reasoning:

```

{
  "inferred_query": "Find the towels hanging on the entrance to the shower.",
  "relevant_objects": [103, 104],
  "query_achievable": true,
  "final_relevant_objects": [103],
  "explanation": "The most relevant object is the toilet with towels
  in bathroom scene (id: 103), which matches the query description."
}.

```

For the same request, our BBQ approach chose a more precisely object that responded to the request, while carrying out the following reasoning:

```

{
  "explanation": "The object 'White towel hanging on rod' (id 53) is the most
  likely candidate because it is described as 'hanging on rod', which matches
  the query's description of 'hangin on the entrance to the shower'.
  Additionally, the object's description does not mention being on the floor or
  on a towel rack, which are common places for towels, but not typically associated
  with being hung on a rod.",
  "id": 53
}.

```

The box selected by our algorithm better matches the request. The result is shown in the image 7 with a blue box.

ConceptGraphs gave an answer to the query of "the suitcase closest to the door", which is shown in the figure 8 with a red bounding box, giving the following reasoning:

```

{
  "inferred_query": "The suitcase closest to the door",
  "relevant_objects": [9, 69, 91],
  "query_achievable": true,
  "final_relevant_objects": [9],
  "explanation": "The suitcase closest to the door is the black suitcase with id 9,
  located in the scene."
}

```

For the same request, our BBQ approach chose a more precisely object that responded to the request, while carrying out the following reasoning:

```

{
  "explanation": "I chose object 37 because it is the only suitcase with a relation
  to the door (id 46) with a pre-computed Euclidean distance, which is 3.52 m.
  This distance is the shortest among all suitcases.",
  "id": 37
}.

```

The box selected by our algorithm better matches the request. The result is shown in the image 8 with a blue box.

ConceptGraphs gave an answer to the query of the trash can that is beside the sink, which is shown in the figure 9 with a red bounding box, giving the following reasoning:

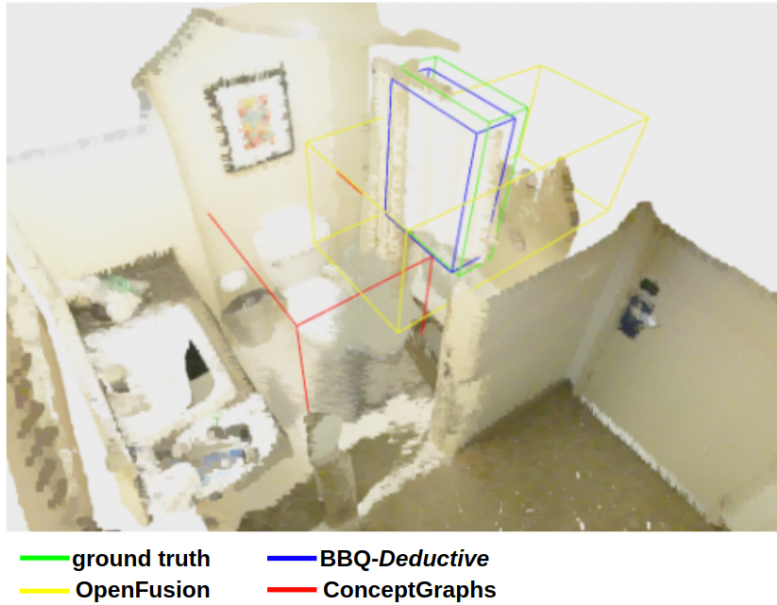


Figure 7: Qualitative analysis of 3D referred object retrieval on the Nr3D datasets was conducted using scene0435\_00. The image on the right displays the outcome of the query for identifying *The towels that are hanging on the entrance to the shower*. The OpenFusion results are indicated by a yellow bounding box, BBQ results by a blue bounding box, Conceptgraphs results by a red bounding box, and the ground truth is marked with a green bounding box.



Figure 8: Qualitative analysis of 3D referred object retrieval on the Nr3D datasets was conducted using scene0435\_00. The image on the right displays the outcome of the query for identifying *the suitcase closest to the door*. The OpenFusion results are indicated by a yellow bounding box, BBQ results by a blue bounding box, Conceptgraphs results by a red bounding box, and the ground truth is marked with a green bounding box.

```
{
  "inferred_query": "the trash can that is beside the sink",
  "relevant_objects": ["109"],
  "query_achievable": true,
  "final_relevant_objects": ["109"],
  "explanation": "The object tag for object 109 is 'large metal trash can',
  which is likely the trash can beside the sink."
}
```

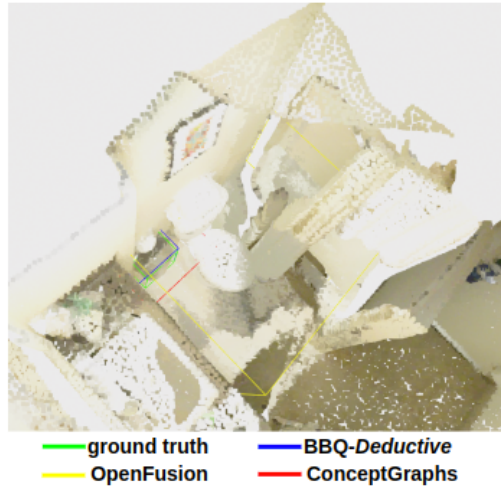


Figure 9: Qualitative analysis of 3D referred object retrieval on the Nr3D datasets was conducted using scene0435\_00. The image on the right displays the outcome of the query for identifying *the trash can that is beside the sink*. The OpenFusion results are indicated by a yellow bounding box, BBQ results by a blue bounding box, Conceptgraphs results by a red bounding box, and the ground truth is marked with a green bounding box.

For the same request, our BBQ approach chose a more precisely object that responded to the request, while carrying out the following reasoning:

```

{
  "explanation": "The object that best corresponds to the query is the one with id 60,
  which is described as 'Trash can with black lid.' It is also mentioned in the 'relations'
  field that this trash can is at a distance of 1.1 m from the White sink with silver
  faucet with id 64, which is a strong indication that it is beside the sink.",
  "id": 60
}.

```